# Subfemtosecond *K*-Shell Excitation with a Few-Cycle Infrared Laser Field

Gilad Marcus*
*Max-Planck-Institut für Quantenoptik, Hans-Kopfermann-Straße 1, 85748 Garching, Germany and Department of Applied Physics, The Benin School of Engineering and Computer Science, The Hebrew University of Jerusalem, Jerusalem 91904, Israel*

Wolfram Helml
*Max-Planck-Institut für Quantenoptik, Hans-Kopfermann-Straße 1, 85748 Garching, Germany*

Xun Gu
*Max-Planck-Institut für Quantenoptik, Hans-Kopfermann-Straße 1, 85748 Garching, Germany*

Yunpei Deng
*Max-Planck-Institut für Quantenoptik, Hans-Kopfermann-Straße 1, 85748 Garching, Germany*

Robert Hartmann
*PNSensor GmbH, Otto-Hahn-Ring 6, 81739 München, Germany*

Takayoshi Kobayashi
*Advanced Ultrafast Laser Research Center, The University of Electro-Communications, 1-5-1, Chofugaoka, Chofu, Tokyo 182-8585, Japan and JST, CREST, K's Gobancho, 7, Gobancho, Chiyoda-ku, Tokyo 102-0076, Japan*

Lothar Strueder
*Max-Planck-Institut für extraterrestrische Physik, Giessenbachstrasse, 85748 Garching, Germany*

Reinhard Kienberger
*Max-Planck-Institut für Quantenoptik, Hans-Kopfermann-Straße 1, 85748 Garching, Germany and Fakultät für Physik, Technische Universität München, James Franck Straße, 85748 Garching, Germany*

Ferenc Krausz
*Max-Planck-Institut für Quantenoptik, Hans-Kopfermann-Straße 1, 85748 Garching, Germany and Department für Physik, Ludwig Maximilians Universität, Coulombwall 1, 85748 Garching, Germany*

(Received 28 September 2010; revised manuscript received 15 March 2011; published 10 January 2012)

Subfemtosecond bursts of extreme ultraviolet radiation, facilitated by a process known as high-order harmonic generation, are a key ingredient for attosecond metrology, providing a tool to precisely initiate and probe ultrafast dynamics in the microcosms of atoms, molecules, and solids. These ultrashort pulses are always, and as a by-product of the way they are generated, accompanied by laser-induced recollisions of electrons with their parent ions. By using a few-cycle infrared ($\lambda_0 = 2.1\ \mu$m) driving laser, we were able to directly excite high-energy ($\sim 870$ eV) inner-shell electrons through laser-induced electron recollision, opening the door to time-resolved studies of core-level and concomitant multielectron dynamics.

DOI: 10.1103/PhysRevLett.108.023201 PACS numbers: 34.80.Dp, 42.50.Hz

Laser-induced electron recollision is a fundamental process at the heart of attosecond science. Insight into this process is provided by a semiclassical three-step model [1,2], in which first the strong electric field of the laser suppresses the atomic Coulomb potential to permit an electron to tunnel out of the atom and gets free with zero initial velocity. After being liberated from the atom, the electron gains energy in the laser field, which, if linearly polarized, pushes the electron first away and then back again towards its parent ion. The outcome of this laser-induced recollision branches into several possible channels, including recombination of the electron with its parent ion followed by the emission of an extreme ultraviolet (XUV) or soft-x-ray photon [via high-order harmonic generation (HHG)] and excitation or secondary ionization of the atom or molecule (via inelastic scattering) [3–5].

For years, time-domain observation of intra-atomic electron dynamics has relied on the presence of a strong laser field, via streaking or tunneling spectroscopy, with a subfemtosecond [6–8] XUV pulse used as a trigger and a strong few-cycle laser field as a probe [5]. Recently, subfemtosecond XUV pulses have also been demonstrated as a probe, permitting real-time measurement of electronic motion in the absence of strong fields [9]. This weak probe

 

nevertheless requires a strong excitation of the interrogated sample which could so far only be provided by multiphoton transitions driven by the synchronized few-cycle-near-infrared pulse. This mechanism can produce only relatively low-energy excitations, restricting real-time probing of electronic phenomena to valence-band or shallow inner-shell excitations [10]. In this Letter, we show evidences that a strong few-cycle IR laser field can produce high-energy inner-shell excitations via laser-induced inelastic electron recollision, which, in combination with the inherently synchronized subfemtosecond XUV probe, paves the way for attosecond real-time observation of electronic processes following inner-shell excitation [11–13].

In our experiments, ensembles of neon atoms (Ne) and nitrogen molecules ($N_2$) were exposed to 17 fs, 350 $\mu$J, few-cycle laser pulses carried at a wavelength of 2.1 $\mu$m with a repetition rate of 1 kHz [14]. The laser beam was focused with a $f = 250$ mm $CaF_2$ lens to a spot size of $\approx 35$ $\mu$m full width at half maximum, measured by a knife-edge scan. Since the kinetic energy of the recolliding electron is proportional to the ponderomotive energy $U_p \sim I\lambda^2$, the long carrier wavelength $\lambda$ together with the short IR pulse allows the production of recolliding electrons with kinetic energies exceeding the $K$-shell binding energy of Ne ($\sim 870$ eV) at comparably low laser intensities $I$, thereby avoiding excessive ionization of the gas [15,16]. The interaction between the laser beam and the gas takes place within a nickel tube with an inner diameter of $\sim 2$ mm. The best harmonic yield was achieved when the laser was focused $\sim 350$ $\mu$m before the center of the tube. At this position, the laser peak intensity was $\sim 1.2 \times 10^{15}$ W/cm$^2$, which, according to the theoretically predicted cutoff harmonic energy $E_c = I_p + 3.17U_p$, is enough to generate harmonics with photon energy above 1 keV ($I_p$ is the ionization potential of the used gas). The soft-x-ray emission from both the coherent HHG process and the incoherent spontaneous decay of the excited atoms was recorded by a custom-made CCD camera (PNSensor GmbH) consisting of $264 \times 264$ pixels (complete detection area $\sim 1$ cm$^2$), each pixel being an independent energy-resolving x-ray detector. In contrast to the well-known metal-oxide-silicon (MOS) based MOSCCDs, *pn*CCDs are based on high-resistivity $n$-type silicon and a manufacturing process which makes use of both wafer surfaces for the sensor and electronics circuitry. This enables a full depletion of the entire silicon volume and thus makes use of the full depth as sensitive volume. Since all components of the sensor are built up with $pn$ junctions instead of MOS structures, the device is denoted *pn*CCD [17,18]. The energy resolution of this camera is about 12%, limited by the Fano factor of silicon. This CCD spectrometer was placed about 60 cm away from the harmonic source, shielded from the IR fundamental light by a 500 nm thick aluminum or magnesium filter, and was calibrated by the insertion of additional thin vanadium and iron filters [see Figs. 1(b) and 1(c)]. Compared with the spectrum transmitted only through the aluminum filter [Fig. 1(a)], a clear cut at the $L$ edges of vanadium and iron in the filtered spectra can be observed. Since noise and scattered light from the laser are always issues to be concerned about, we performed two control experiments to confirm that the recorded spectrum is indeed coming from the laser-gas interaction. In the first test, we used the laser at the same conditions as we did with the harmonic generation but switched the gas flow off. In the second test, we run the harmonic generation experiment with the gas flow on but with a glass window in front of the *pn*CCD. In both control tests, the harmonic spectra vanished. Another source of errors to be concerned about is a case in which two photons hit the same pixel at the same time, leading to overestimation of the photon's energy. We checked this kind of error and found it to be negligible. More information about this error and the *pn*CCD is found in the Supplemental Materials [19].

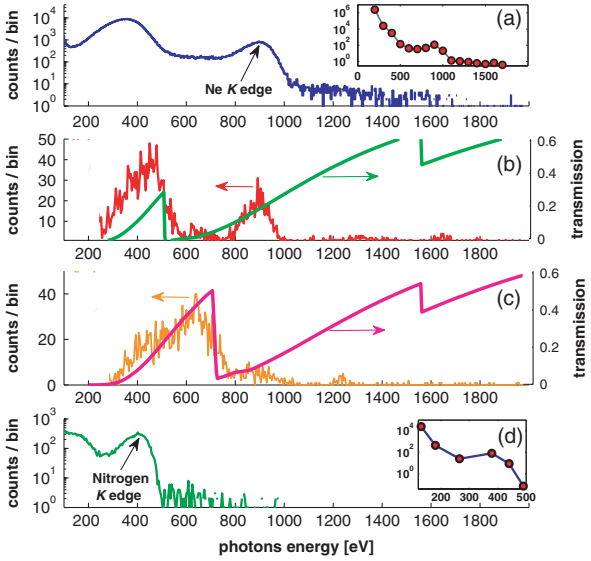


FIG. 1 (color). High-harmonic spectrum generated with (a) Ne and (d) $N_2$. (b) and (c) show the HHG spectra of Ne through an additional 500 nm of vanadium and iron filters, respectively. Comparing the spectra in (b) and (c) to the spectrum in (a), a clear cut can be seen at the vanadium and iron $L$ edges. The transmission curves of the vanadium and iron filters are presented, as well, as green and pink lines. The insets in (a) and (d) show the averaged absolute photon count rate (photons/ sec ) in a 10% bandwidth, taking into account the transmission of the filters and the spectrometer efficiency.

Figures 1(a) and 1(d) show typical spectra obtained with Ne through a 500 nm aluminum filter and with $N_2$ through a 500 nm magnesium filter under identical conditions of laser irradiation and integrating over $2.6 \times 10^5$ laser pulses. Qualitatively, they look similar: both exhibit a plateau, extending up to the $K$ edge of the target atom ($\sim 870$ eV for Ne, $\sim 410$ eV for $N_2$), followed by a sharp drop at the $K$ edge. In both cases, we observed a

distinctive peak around the $K$ edge (the other peak at the lower end of the spectrum is an artifact due to the high absorption of the aluminum or magnesium filters below 200 eV). The independent occurrence of pronounced peaks around the $K$ edge, both in Ne and $N_2$, strongly suggests that an additional inner-shell process is involved here.

To exclude the possibility that merely favorable phase-matching conditions, caused by the sharp change in the index of refraction at the $K$-absorption edge, give rise to the observed spectral enhancement, we take a closer look at this process. Phase-matching occurs when the coherent radiation from each target atom adds constructively, so that the harmonic yield grows quadratically with the number of emitters. Such a coherent buildup occurs in HHG, provided the phase velocity of the harmonics matches that of the fundamental laser pulse. In mathematical form, it requires that $\Delta k_q = (k_q - qk_0) = 0$, where $k_0$ is the wave vector of the driving laser and $k_q$ is the $q$th harmonic wave vector. The phase mismatch is composed of the sum of the dispersion difference stemming from the neutral gas atoms, the dispersion difference induced by the plasma created by the laser, and a purely geometrical factor known as the Gouy phase shift [20]. It can be written as $\Delta k_q = qk_0(\delta n_{\text{atom}} + \delta n_{\text{plasma}} - 1/k_0 z_R)$, where $\delta n_{\text{atom,plasma}} = n_q - n_0$ is the difference between the respective refraction indices at the $q$th harmonic and the fundamental wavelength and $z_R$ is the Rayleigh range. Under our experimental conditions and for harmonics around 870 eV, we can estimate these contributions (neglecting, for the moment, possible resonance effects in the x-ray regime) as $\Delta k_{\text{atom}} \approx -3.5 \times 10^3\ \text{cm}^{-1}$, $\Delta k_{\text{plasma}} \approx 5 \times 10^5\ \text{cm}^{-1}$, and $\Delta k_{\text{Gouy}} \approx -7.3 \times 10^3\ \text{cm}^{-1}$. Here, we find that the plasma dispersion dominates over the other contributions by 2 orders of magnitude, thus allowing only for a low efficiency of HHG.

Next, we investigate whether the influence of a nearby resonant transition can improve the phase-matching. Around a resonance line, the index of refraction may be written as $n^2 = 1 + A(\omega_0^2 - \omega^2 - i\omega\gamma_0)^{-1}$ and the radiation wave vector may be approximated as $k = \beta + i\alpha/2 \approx 1 + (A/2)(\omega_0^2 - \omega^2 - i\omega\gamma_0)^{-1}$, where $A$ is proportional to the oscillator strength, $\omega_0$ and $\gamma_0$ are the frequency and the natural width of the resonance transition, $\beta$ is the real part of the wave vector, and $\alpha$ is the absorption coefficient. By substituting the values for $\alpha$, $\omega_0$, and $\gamma_0$ [21], we calculated that the maximum value for $(1 - n_{\text{atom}})$ in the XUV around the resonance is about $10^{-6}$, which is still 2 orders of magnitude lower than the values of $(1 - n_{\text{atom}})$ in the near-IR regime. Therefore, we conclude that the resonance transition around the $K$ edge can not account for a dramatic change in the phase mismatch factor.

The other possibility to explain the enhanced peak around the $K$ edge is that, once the recolliding electrons have enough energy to excite inner-shell electrons in their parent ions, the excited ions may subsequently decay via Auger electron emission or x-ray fluorescence. This incoherent x-ray photon emission may explain the enhanced feature we observed around the $K$-edge regions. Support for this hypothesis is gained by analyzing the XUV beam profile as a function of the photon energy. It is well-known that the harmonics beam, due to its spatial coherence, has a very low divergence and well-defined beam shape. The fluorescent radiation, on the other hand, is going into all directions and is expected to cover the detector uniformly. The ability of our custom-built detector to resolve both the position and the energy of the XUV photons at the same time allows us to observe the shape of the emitted radiation as a function of the photon energy. Figure 2 shows the energy-resolved XUV radiation profiles at two different spectral ranges. The first profile is taken at the spectral range between 200–400 eV, where the XUV radiation is expected to come from the harmonic process, while the second profile is set in the spectral range between 750–950 eV, around the $K$ edge of Ne, where we assume that the radiation is coming mainly from fluorescence. Although not perfectly aligned through the aluminum filter and on the CCD chip, we clearly see that the radiation between 200–400 eV is spatially confined, as we can expect from high-harmonic radiation. On the other hand, the radiation distribution in the spectral range between 750–950 eV is uniform, supporting the assumption that it stems from a fluorescence process.

To further verify whether this conjecture applies, we scrutinized the pressure dependence of the photon yield (see details in the Supplemental Materials [19]) and, in particular, around the $K$ edge. The probability per unit time for an electron detached at $t = t_i$ to excite an inner-shell electron of its parent ion is given by

$$dp_{ex}(t_i) = (\sigma_{ie}/\pi W^2)\eta(t_i)dt, \tag{1}$$

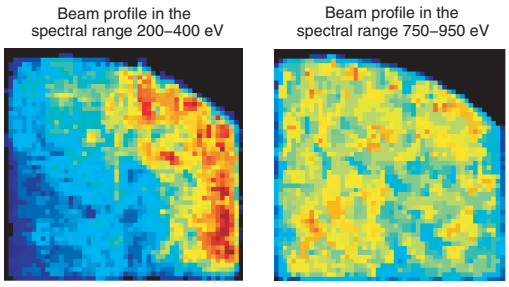


FIG. 2 (color). Energy-resolved XUV radiation profiles for two different spectral ranges. The uniform radiation distribution at photon energies of 750–950 eV is an indication that it comes from a fluorescence process and not from harmonic generation. The detector size is $\sim 1 \times 1$ cm and it was placed 60 cm away from the gas target. The rounded upper-right corner is due to the aluminum filter.

where $\sigma_{ie}$ is the cross section for excitation of the inner-shell electron through inelastic collision, $W$ is the radius of the electron wave packet at the recollision time, and $\eta$ is the ionization rate calculated with the Ammosov-Delone-Krainov tunnel ionization theory [22]. The density of the excited ions is accordingly $\rho_{ex} = \int \rho_0 dp_{ex} = \rho_0 \frac{\sigma_{ie}}{\pi W^2} R$, where $\rho_0$ is the gas density and $R = \int \eta(t) dt$ is the total degree of ionization. Including also the self-absorption in the gas, we can write the differential equation for the emitted photons as $dN/dz = \rho_{ex} S - (R\rho_0\sigma_a)N$, where $N$ is the number of photons, $z$ is the spatial coordinate in the direction of the laser propagation, $S$ is the effective beam area in which the local intensity is high enough to generate electrons with energies above the $K$ edge, and $\sigma_a$ is the absorption cross section. By solving this equation, we finally get the averaged photon count rate on the CCD:

$$\Phi_{av} = \frac{\rho_{ex}}{R\rho_0} \frac{S}{\sigma_a} [1 - \exp(-R\rho_0\sigma_a L_{\mathrm{med}})] \frac{\Gamma_{\mathrm{rad}}}{\Gamma_{\mathrm{Au}}} f_R \frac{d\Omega}{4\pi}. \quad (2)$$

Here, $L_{\mathrm{med}}$ is the length of the interaction medium; $\Gamma_{\mathrm{rad}}$ and $\Gamma_{\mathrm{Au}}$ are the x-ray radiation and the Auger decay rate of the excited state, respectively; $f = 1$ kHz is the laser repetition rate; and $d\Omega$ is the solid angle subtended by the CCD. Because of the limited resolution of our spectrometer and in order to simplify our model, we choose only the $1s^1 2s^2 2p^6 \rightarrow 1s^2 2s^2 2p^5$ transition, although the proposed mechanism may initiate many different excited states or excited ions which will decay through a variety of channels. Nevertheless, the cross sections for all these channels are within the same order of magnitude. A single fitting parameter ($\sigma_{ie}$) has been used to compensate for this uncertainty. Furthermore, a change in any of the less well-defined parameters ($\sigma_{ie}$, $\eta(t)$, $\Gamma_{\mathrm{rad}}$, and $S$) causes merely a rescaling, thus not compromising our general argument. Since $\rho_{ex} \propto \rho_0$, Eq. (2) predicts a linear growth of the photon yield with the pressure, followed by a saturation when $(R\rho_0\sigma_a)L_{\mathrm{med}} \gg 1$ (see inset of Fig. 3). By substituting the absorption cross section and the gas density relevant to our experiment (Table 1 in the Supplemental Materials [19]), we find that the predicted photon yield should already be saturated in a pressure region, where our experimental data still show a linear growth (see Fig. 3).

In an attempt to elucidate this behavior further, we have to expand our model to include electron collisions with neighboring atoms, on account of the fact that, due to the long driver wavelength, the liberated electron's excursion amounts to a few tenths of nanometers, making the probability of collision with neighboring atoms at high pressures significant. This can be taken into account by replacing (1) with $dp_{ex}(t_i) = [\eta(t_i)dt] \int_{t_i}^{\infty} \rho_0 \sigma_{ie}(v) v(t') dt'$ and accordingly rewriting the differential equation for the photon emission $dN/dz = \rho_{ex} S - [(1 - R)\rho_0\sigma_a]N$, where $v(t)$ is the velocity of the electron in the laser field and $\rho_{ex} = \int \rho_0 dp_{ex}$ is obtained by substituting the new excitation probability $dp_{ex}$. Here, we assumed the transition $1s^1 2s^2 2p^6 3p^1 \rightarrow 1s^2 2s^2 2p^6$, although it is again only a representative transition, and $\sigma_{ie}$ was used as a fitting parameter. Using the experimental parameters given in Table 1 of the Supplemental Materials [19], we obtain a theoretical prediction in excellent agreement with the experimental data (see Fig. 3). We note that we have neglected the contribution of the coherent radiation in all of the above calculations. This is justified, regarding the observed decrease of the coherent photon yield by an order of magnitude in the range between 500–700 eV [see Fig. 1(a)] and our previous calculation that we cannot expect better phase-matching conditions in this energy range. Our results (comparison of the blue and red curves in Fig. 3) therefore reveal that, for high pressures, collisions with neighboring atoms become the dominant inner-shell excitation mechanism in our case.

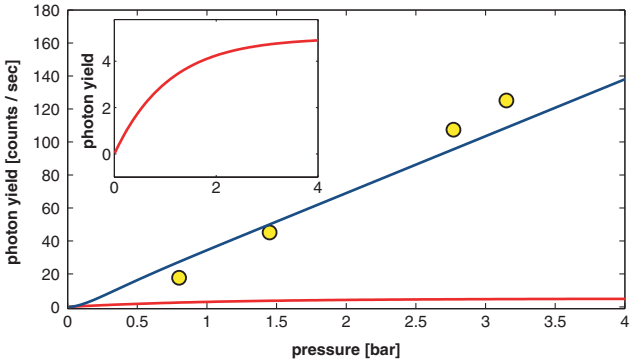


FIG. 3 (color). The photon yield around the Ne $K$ edge as a function of the backing pressure of the target gas. The red lines in the main figure and in the inset show the predicted incoherent photon yield according to the model of recollision with the parent ion; the blue line represents the prediction of the expanded calculation, taking into account the collisions with neighboring atoms. The yellow circles mark the measured photon yield at a 10% bandwidth around 870 eV (resulting from both coherent and incoherent radiation).

In conclusion, the enhanced peak and the isotropicity of the XUV radiation at the spectral range around the $K$ edge are evidence for inner-shell excitation by the laser-induced electron recollision. Owing to the highly nonlinear scaling of the tunneling probability with laser intensity and the few-cycle pulse duration, the excitation can be substantially confined to a single, isolated recollision event and hence to a tiny fraction of the laser oscillation period. The resultant subfemtosecond trigger window and the orders-of-magnitude enhanced excitation probability (as compared to the use of current generation high-harmonic sources) open the prospect for studying a plethora of atomic and molecular inner-shell excitation and relaxation processes directly in the time domain [12].

R. K. acknowledges funding from the Alexander von Humboldt Foundation and the ERC Starting Grant.

*marcus@vms.huji.ac.il.

[1] J. L. Krause, K. J. Schafer, and K. C. Kulander, Phys. Rev. Lett. **68**, 3535 (1992).
[2] P. B. Corkum, Phys. Rev. Lett. **71**, 1994 (1993).
[3] D. N. Fittinghoff, P. R. Bolton, B. Chang, and K. C. Kulander, Phys. Rev. Lett. **69**, 2642 (1992).
[4] M. F. Kling, C. Siedschlag, A. J. Verhoef, J. I. Khan, M. Schultze, T. Uphues, Y. Ni, M. Uiberacker, M. Drescher, F. Krausz, and M. J. J. Vrakking, Science **312**, 246 (2006).
[5] F. Krausz and M. Ivanov, Rev. Mod. Phys. **81**, 163 (2009).
[6] I. P. Christov, M. M. Murnane, and H. C. Kapteyn, Phys. Rev. Lett. **78**, 1251 (1997).
[7] M. Hentschel, R. Kienberger, C. Spielmann, G. A. Reider, N. Milosevic, T. Brabec, P. Corkum, U. Heinzmann, M. Drescher, and F. Krausz, Nature (London) **414**, 509 (2001).
[8] E. Goulielmakis, M. Schultze, M. Hofstetter, V. S. Yakovlev, J. Gagnon, M. Uiberacker, A. L. Aquila, E. M. Gullikson, D. T. Attwood, R. Kienberger, F. Krausz, and U. Kleineberg, Science **320**, 1614 (2008).
[9] E. Goulielmakis, Z. Loh, A. Wirth, R. Santra, N. Rohringer, V. S. Yakovlev, S. Zherebtsov, T. Pfeifer, A. M. Azzeer, M. F. Kling, S. R. Leone, and F. Krausz, Nature (London) **466**, 739 (2010).
[10] M. Drescher, M. Hentschel, R. Kienberger, M. Uiberacker, V. Yakovlev, A. Scrinzi, T. Westerwalbesloh, U. Kleineberg, U. Heinzmann, and F. Krausz, Nature (London) **419**, 803 (2002).
[11] E. Seres, J. Seres, and C. Spielmann, Appl. Phys. Lett. **89**, 181919 (2006).
[12] P. B. Corkum and F. Krausz, Nature Phys. **3**, 381 (2007).
[13] N. Milosevic, P. B. Corkum, and T. Brabec, Phys. Rev. Lett. **92**, 013002 (2004).
[14] X. Gu, G. Marcus, Y. Deng, T. Metzger, C. Teisset, N. Ishii, T. Fuji, A. Baltuška, R. Butkus, V. Pervak, H. Ishizuki, T. Taira, T. Kobayashi, R. Kienberger, and F. Krausz, Opt. Express **17**, 62 (2009).
[15] J. Tate, T. Auguste, H. G. Muller, P. Salieres, P. Agostini, and L. F. DiMauro, Phys. Rev. Lett. **98**, 013901 (2007).
[16] P. Colosimo, G. Doumy, C. I. Blaga, J. Wheeler, C. Hauri, F. Catoire, J. Tate, R. Chirla, A. M. March, G. G. Paulus, H. G. Muller, P. Agostini, and L. F. DiMauro, Nature Phys. **4**, 386 (2008).
[17] R. Hartmann, K. H. Stefan, and L. Strüder, Nucl. Instrum. Methods Phys. Res., Sect. A **439**, 216 (2000).
[18] R. Hartmann, W. Buttler, H. Gorke, and L. Strüder, *et al.*, Nucl. Instrum. Methods Phys. Res., Sect. A **568**, 118 (2006).
[19] See Supplemental Material at http://link.aps.org/supplemental/10.1103/PhysRevLett.108.023201 for (a) description of the *pn*CCD and error reading analysis, (b) details about the pressure dependence of the high harmonics, and (c) a table of parameters.
[20] P. Balcou, P. Salières, A. L'Huillier, and M. Lewenstein, Phys. Rev. A **55**, 3204 (1997).
[21] T. E. Glover, M. P. Hertlein, S. H. Southworth, T. K. Allison, J. van Tilborg, E. P. Kanter, B. Krassig, H. R. Varma, B. Rude, R. Santra, A. Belkacem, and L. Young, Nature Phys. **6**, 69 (2010).
[22] M. V. Ammosov, N. B. Delone, and V. P. Krainov, Sov. Phys. JETP **64**, 1191 (1986).